Scanning Microscopy

Volume 1990
Number 4 *Fundamental Electron and Ion Beam Interactions with Solids for Microscopy, Microanalysis, and Microlithography*

Article 17

1990

# Angular and Energy Distributions of Electrons Emitted from Gases and Thin Foils During Light Ion Bombardment

L. H. Toburen
*Pacific Northwest Laboratory, Washington*

**Scanning Microscopy Supplement 4, 1990 (Pages 239-256)**
Scanning Microscopy International, Chicago (AMF O'Hare), IL 60666 USA

0892-953X/90$3.00+.00

# ANGULAR AND ENERGY DISTRIBUTIONS OF ELECTRONS EMITTED FROM GASES AND THIN FOILS DURING LIGHT ION BOMBARDMENT

L. H. Toburen

Pacific Northwest Laboratory
P.O. Box 999 (P8-47)
Richland, Washington 99352

Telephone: (509) 376-3348

## Abstract

The energy and angular distributions of electrons ejected by fast charged particles in ionizing collisions provide detailed information regarding the effects of atomic, molecular, and condensed-phase structure on the energy loss process. Analysis of the wide range of available data has lead to several general conclusions. For ionization of atomic and molecular targets by protons having energies above a few hundred keV, the cross sections for electron production have been found to scale as the number of loosely bound target electrons. The more subtle features of the ejected electron energy spectra are, however, dependent on the electronic structure of the target, especially for emission of low-energy electrons. Although ab initio theoretical techniques are currently limited to simple systems, cross sections for electron production in collisions of bare charged particles with atomic targets can be reliably calculated using Born theory. For more complex targets, models have been developed that provide singly-differential electron-emission cross sections for a wide range of ion energies. These models rely on experimental data to determine parameters that are difficult or infeasible to obtain by ab initio theory. Although great strides have been made in understanding ionization processes involving bare ions and atomic and molecular targets, understanding the collision process for structured ions, i.e., ions that carry bound electrons, as well as collision processes in solid targets, presents a greater challenge. With structured ions, the screening of the ion's nuclear charge by its bound electrons results in an effective interaction potential that depends on the collisional energy loss. In addition, this screened potential has been found to vary with energy loss in a functionally different manner for different light ions. For solid targets, differential ionization cross sections for ion impact are fragmentary, and theoretical results exhibit only qualitative agreement.

Keywords: ionization, differential cross sections, proton impact, light ion impact, foil targets, atomic and molecular targets.

## Introduction

Secondary electron emission produced by interactions of charged particles with atomic, molecular, and condensed-phase targets plays an important role in a wide range of research fields. These electrons are responsible for the spatial structure of charged-particle tracks and lead to variations in the relative biological effectiveness (RBE) of high linear-energy-transfer (LET) radiation. This same track structure leads to LET-dependent soft error upset in electronic microcircuits and ion-induced damage in materials. The transport of secondary electrons is also responsible for a large fraction of the electrons emitted from surfaces by ion bombardment, which is important in a number of practical applications such as microscopy and particle detection. Because ionization is the primary means of energy loss by fast charged particles, absolute cross sections for the production of secondary electrons can provide detailed information on the energy loss process.

A number of reviews have been published describing secondary electron emission cross sections that are differential in ejected electron energy and angle for ionization of atomic and molecular targets by light ions; see, for example, Berenyi (1987), Toburen (1982), Stolterfoht (1978), Rudd (1975), and Ogurtsov (1972). An excellent review of secondary electron emission from bombardment of surfaces by electrons and protons has recently been published by Schou (1988). The theory of electron transport in solids has also been reviewed by Schou (1980). In this paper, a brief review will be presented of the general features observed in measured cross sections for emission of electrons, differential in ejected electron energy and emission angle, for collisions of light ions with atoms, molecules, and solids. The effects of target and projectile structure on the ejected electron spectra will be presented, and model calculations that have been developed to describe singly differential electron emission cross sections will be discussed. Finally, electron emission cross sections observed for solid targets will be compared with similar data from gas targets. The purpose of this review is to provide a guide to the basic features of the data and to provide references that will enable the interested reader to seek further information. It would be impossible to present a detailed review of the entire field in a brief paper.

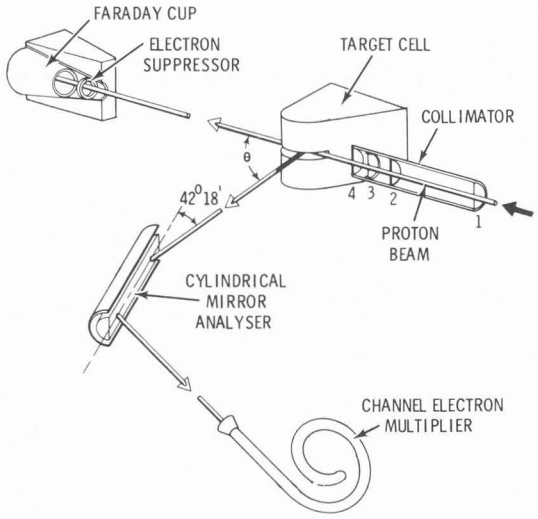


Fig. 1. Apparatus used at Pacific Northwest Laboratory for doubly differential electron emission cross section measurements. For detailed description see Toburen (1971).

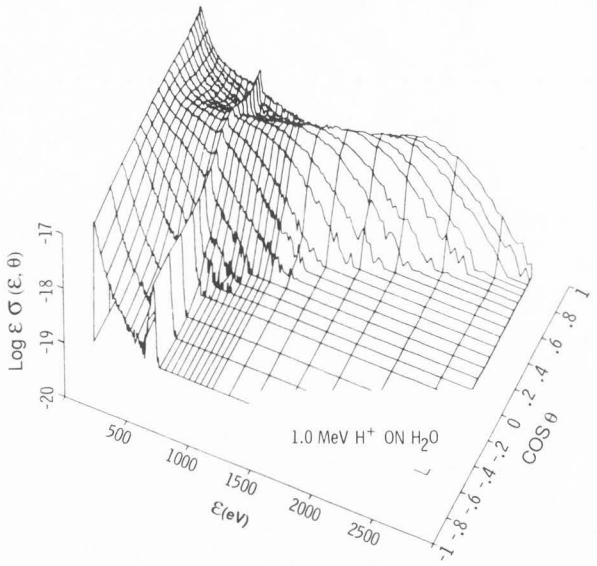


Fig. 2. Energy and angular distribution of electrons ejected from water vapor by 1.0-MeV protons. Data are from Toburen et al. (1980).

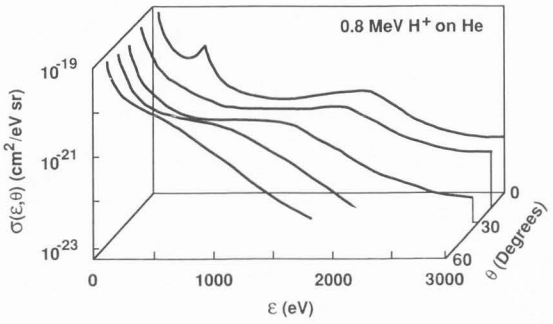


Fig. 3. Electron emission at small angles for 0.8-MeV protons in collision with helium gas. Data are from Schader et al. (1984).

## Interactions Involving Bare Ions

### Instrumentation

The majority of the experimental work conducted to investigate doubly differential cross sections for electron production has been undertaken with bare ions, and most of these studies have focused on proton impact. Reviews of these data have been published by Berenyi (1987), Toburen (1982), Stolterfoht (1978), Rudd (1975), and Ogurtsov (1972). In addition an extensive data compilation has been published by McDaniel et al. (1979). The studies of continuum electron emission have been largely the work of research groups at the Pacific Northwest Laboratory (Toburen), the University of Nebraska (Rudd), and Hahn-Meitner Institute (Stolterfoht). Auger electron spectroscopy in ion-atom collisions has also been an active field of investigation in these as well as other laboratories. A discussion of Auger electron spectroscopy is, however, considered outside the scope of this article; the interested reader is directed to a recent review by Stolterfoht (1987).

A schematic drawing of the apparatus used for measurements of doubly differential electron emission cross sections at the Pacific Northwest Laboratory (PNL) is shown in Fig. 1; it has been described in detail by Toburen (1971). The basic components of the apparatus include an incident beam collimator, a differentially pumped target gas cell, a shielded and biased Faraday cup for beam intensity determination, a cylindrical-mirror electrostatic analyzer for electron energy analysis, and a continuous-channel electron multiplier for electron detection. The entire apparatus is housed in a vacuum chamber designed so that the electron analyzer can be remotely rotated around the target cell to detect electrons at different emission angles. Residual magnetic fields are minimized by means of three mutually perpendicular Helmholtz coils. Similar systems have been used at other laboratories; major differences consist of the type of electrostatic analyzer, the type of gas target and the method of magnetic field nullification. The Hahn-Meitner studies (Stolterfoht, 1971) employed a parallel-plate electrostatic energy analyzer, a gas beam target, and magnetic field nullification by means of mu-metal shielding. At the University of Nebraska, a 127° electrostatic energy analyzer was used, with a static gas target, and Helmholtz coils for magnetic field nullification (Rudd and Jorgensen, 1963), (Crooks and Rudd, 1971), (Rudd, 1975).

### Spectral Features

An example of the data obtained with the PNL system is shown in Fig. 2 for ionization of water vapor by 1-MeV protons (Toburen and Wilson, 1977). The basic features of the spectra are a maximum in the cross sections for low-energy electron emission, a broad ridge for emission of fast electrons into angles less than 90°, and a relatively sharp ridge running through the surface at approximately 500 eV. The broad ridge is produced from direct binary collisions between the proton and bound

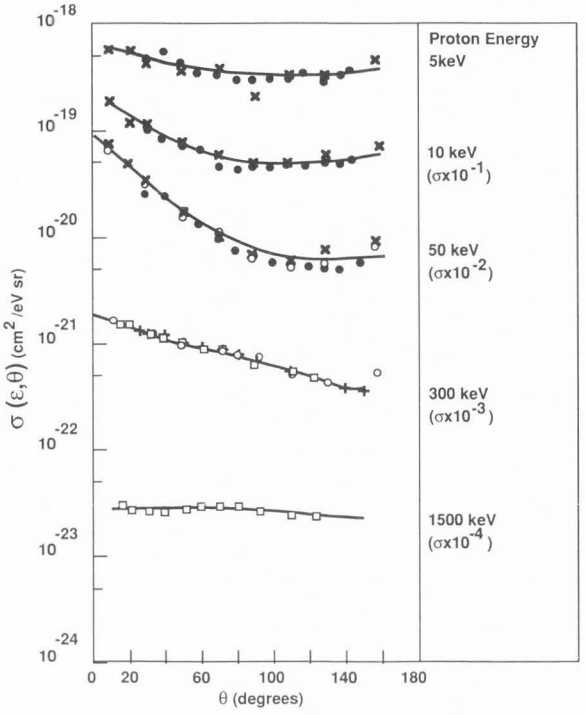


Fig. 4. Angular distributions of 10-eV electrons ejected from argon by protons of different energies. Data are from (●) Criswell et al. (1977), (x) Rudd (Criswell et al. 1977), (o) Crooks and Rudd, (1971), (+) Gabler (1977), and (□) Toburen et al (1978); all data were taken from Rudd et al. (1979).

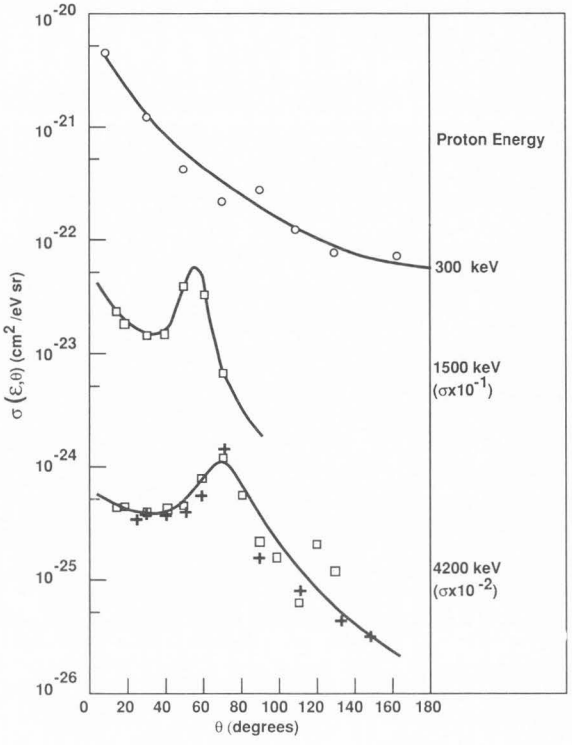


Fig. 5. Angular distributions of 1000-eV electrons ejected from Ar by protons of different energies. Data are from (o) Crooks and Rudd (1971), (□) Toburen et al. (1978), and (+) Gabler (1974); all data were taken from Rudd et al. (1979).

electrons, whereas the sharp ridge at 500 eV is produced by Auger electron emission following K-shell ionization of the oxygen atom of the water molecule. Also apparent in the surface generated by these spectra is a modest increase in the cross sections with decreasingly small angles for electron energies near 500 eV. This increase is attributed to a process called charge-transfer-to-continuum states. This process, first explored by Crooks and Rudd (1970), has been the object of extensive study. Continuum-charge-transfer can be viewed as a process in which an electron is captured into a continuum state of the passing ion. Therefore the major contribution to the ejected electron spectrum is expected at emission angles near 0° for electron energies such that the ejected electron and outgoing proton have comparable velocity. The continuum-charge-transfer peak is clearly seen in the 0° electron spectrum obtained in the work of Schader, et al. (1984) and shown in Fig. 3.

The electron spectra between the continuum-charge-transfer peak and the low energy maximum have also been the subject of extensive study. Electrons ejected in this region are subject to the Coulomb field of both the departing ion and the stationary target ion. Electrons from this portion of the spectrum, referred to as two-center, saddle-point, or Wannier-Ridge electrons, have recently been investigated in high-energy heavy-ion collisions by Stolterfoht et al. (1987) and for low energy protons by Meckbach et al. (1986). A peak in the spectra for electrons ejected with velocity comparable to the bombarding ion has also been observed at small angles in electron emission spectra from solid targets. In the case of solid targets, the mechanism responsible for this peak is somewhat different from that discussed above for gas targets, owing to the density of electronic states in the media. In condensed media, electrons are viewed as becoming trapped in the "wake" produced by the Coulomb potential of the moving charged particle (Neelavathi et al. 1974). These electrons then exit the surface with velocities comparable to that of the moving ion. They are commonly referred to as "convoy electrons" and a number of research groups are actively studying their characteristics; see, for example, Breinig et al. (1982), Yamazaki et al. (1984), Latz et al. (1984) and Focke et al. (1984).

Cross-section Systematics

The trends in the angular distributions of 10-eV and 1000-eV electrons ejected from argon gas by various incident proton energies are illustrated in Figs. 4 and 5, respectively. The angular distributions for ejection of 10-eV electrons, shown in Fig. 4, are nearly isotropic at the highest and lowest proton energies. A relatively isotropic emission is generally observed for low-energy electrons ejected by fast ions. For the intermediate energy protons of Fig. 4 the increase

in the cross sections at small angles is attributed to an enhancement in the cross sections by the continuum-charge-transfer process. As discussed above, this process is most important for ejection of electrons into small angles for electron energies where the ejected electron velocity is comparable to the proton velocity. The 10-eV electrons have a velocity equal to that of a proton with energy of approximately 20 keV, thus the maximum contribution would occur between the 10- and 50-keV data shown. The data for high-energy electron emission, shown in Fig. 5, exhibit peaks in the angular distributions for the 1500-keV and 4200-keV protons. This reflects the nature of direct binary collisions between the incoming proton and the bound electron. The position of the peak can be predicted from simple kinematics of the collision of a proton with a free electron. The width of the peak reflects the initial velocity distribution of the bound target electrons. For the case of 1000-eV electrons ejected by 300-keV protons, shown in Fig. 5, no binary encounter peak is observed; this energy is greater than the most energetic electron that could be ejected by a collision involving 300-keV protons based on simple kinematic arguments.

The data that are plotted in figures 4 and 5 illustrate the extent of agreement among measurements of different laboratories, using different experimental techniques. This agreement is particularly impressive considering that the measurements were independent determinations of <u>absolute</u> cross sections. These data for proton impact ionization of argon are available in tabular form in a compilation by Rudd et al. (1979).

The effects of target molecular structure on proton-induced electron emission cross sections were first investigated by Wilson and Toburen (1975) for simple hydrocarbon molecules. They showed that one could obtain "universal" cross sections for all the molecules investigated (except molecular hydrogen) by simply dividing the cross sections by the number of weakly bound electrons. Weakly bound electrons were defined as all target electrons except the carbon K-shell electrons. This reflects the fact that the proton interacts primarily with the outer shell, or valance, electrons. In Fig. 6 are plotted PNL data for a number of nonhydrogenous molecules, of low-Z elements, and hydrogen, scaled according to the number of weakly bound electrons. The cross sections from targets of $O_2$, $N_2$, $H_2O$, $N_2O$, CO, and $CO_2$ scaled in this way all fit within the cross hatched bands. Hydrogen alone diverges from this systematic representation.

If one were to include the scaled hydrocarbon cross sections of Wilson and Toburen (1975) in Fig. 6, those results would look very similar to the nonhydrogenous molecular data shown there. The scaled hydrocarbon results agree closely with those for the nonhydrogenous molecules at both large and small emission angles, but are slightly higher at the binary encounter peaks, e.g., in closer agreement with $H_2$ data. Without much error, however, one can represent the angular distributions of all the simple molecules (except hydrogen) by universal curves parameterized as a function of ejected electron energy. This similarity of doubly differential cross sections for electron emission from molecular targets makes it

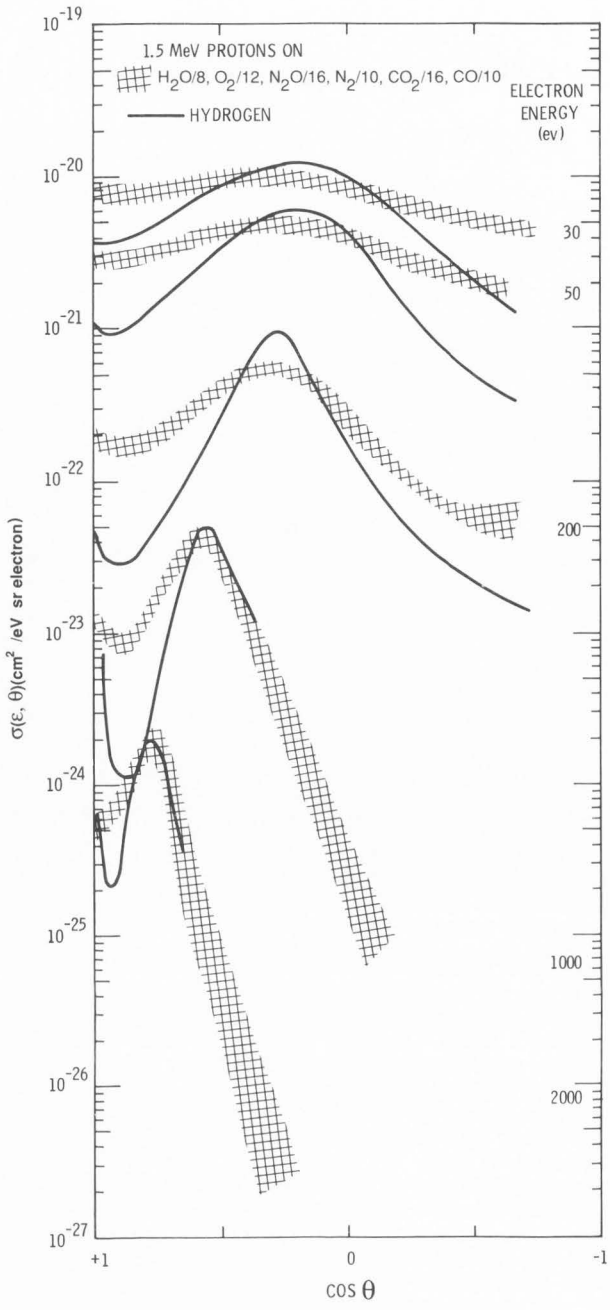


Fig. 6. Angular distributions for several gas targets compared with data for molecular hydrogen. Cross sections were divided by number of outer-shell electrons for comparison of different molecules. Water vapor and oxygen results are from Toburen and Wilson (1977); other results are unpublished Pacific Northwest Laboratory data.

reasonably straightforward to include such data in Monte Carlo models of electron transport.

By integrating the doubly differential cross sections with respect to emission angle, the differential cross sections for energy loss to secondary electrons are obtained. Such singly differential cross sections for ionization of

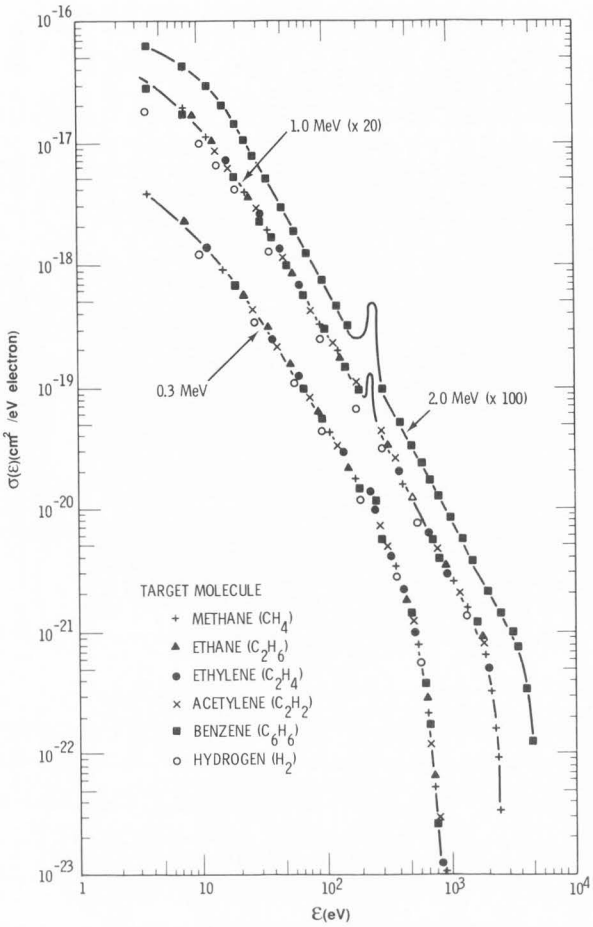


Fig. 7. Single differential cross sections for electron ejection from hydrocarbon molecules and hydrogen for different proton energies. Cross sections divided by number of outer-shell electrons for comparison of different molecules. Data are from Wilson and Toburen (1975).

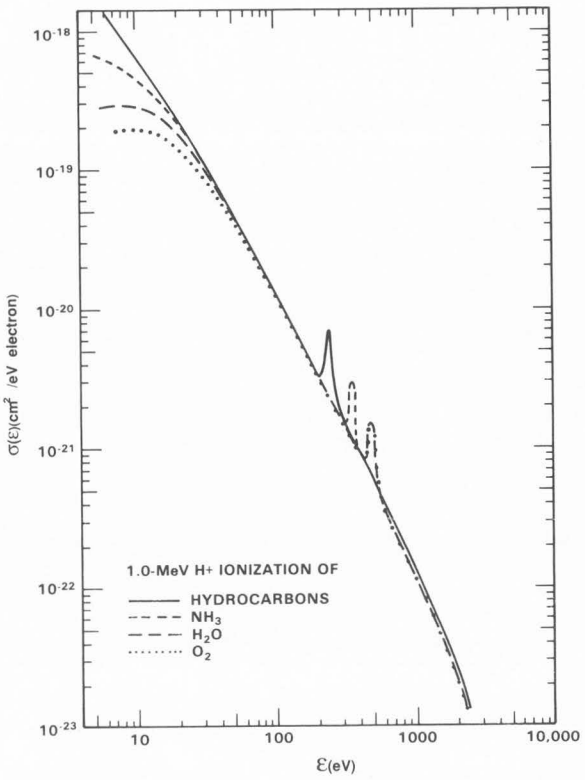


Fig. 8. Single differential cross sections for a number of different molecules. Cross sections were divided by number of outer-shell electrons for comparison of different molecules. Data are from Wilson and Toburen (1975), $H_2O$; Lynch et al. (1976), $NH_3$; Toburen and Wilson (1977), $H_2O$ and $O_2$.

several hydrocarbons by proton impact are shown in Fig. 7, scaled according to the number of weakly bound electrons in the target molecule. Note that singly differential cross sections for electron emission from hydrogen are also in good agreement with the hydrocarbon results. Extending this comparison of singly differential cross sections to other molecules shows effects that are due to the electronic structure of the target. In Fig. 8, a considerable difference is evident in the shape of the low-energy part of the electron emission spectra for the various molecular targets As expected, it is the low energy portion of the electron spectra that reflects differences in the electronic structure of the target. The peaks superimposed on the spectra at approximately 250 eV, 365 eV, and 500 eV are from Auger electrons emitted following K-shell vacancy production in carbon, nitrogen, and oxygen constituents of the molecules, respectively.

Effects of Target Structure

To further investigate the effects of target structure in the low-energy portion of the ejected electron spectra, the apparatus shown in Fig. 1 was modified by replacing the electrostatic analyzer with a time-of-flight (TOF) spectrometer (Toburen and Wilson, 1975). The TOF spectrometer was capable of reliable measurements of electron spectra for electron energies as low as 0.5 eV. Electrostatic analyzers more commonly used for absolute cross section measurements may become unreliable at energies below about 20 eV because of the effects of residual electric and magnetic fields. Data obtained with the TOF technique are shown in Figs. 9-11 to illustrate the influence of target structure on the electron emission spectra. In Fig. 9, spectra recorded at 130° with respect to the direction of the proton beam, normalized in intensity at an ejected electron energy of approximately 500 eV, are compared for several gas targets. In general, the shape of the spectra are similar, with differences in yields at the lower electron energies. An exception is the clearly different shape of the argon spectrum. The rapid decrease in the argon spectrum above about 10-eV is because of the relatively unique atomic structure for noble gas atoms. This is described theoretically as occurring when the matrix element for the $3p \rightarrow \epsilon d$ transition changes sign on passing through zero (Kennedy and Manson, 1972). The corresponding photoionization cross sections for this transition are shown for comparison. Even

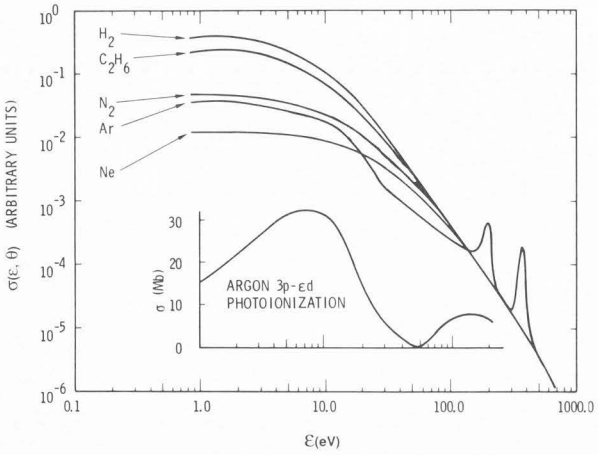


Fig. 9. Low-energy portion of ejected electron spectra for several atoms and molecules. Data (Toburen and Manson, 1975) are for electrons ejected at 130° by 1-MeV protons. Photoionization spectrum is from a calculation of Kennedy and Manson (1972).

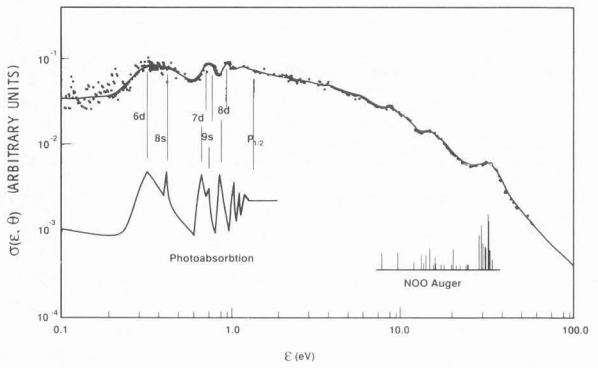


Fig. 10. Low-energy portion of spectrum for electron ejection from Xe at 90° by 1-MeV protons. Photoionization data are from Comes et al. (1968); NOO Auger assignments are from Siegbahn et al. (1969).

though the spectrum of continuum electrons is the sum of electrons from all ionization channels, the 3p→εd ionization channel is sufficiently excited by fast protons to dominate the shape of the observed electron emission spectrum.

Target atomic structure is also reflected in the electron spectrum for xenon, shown in Fig. 10. Here we see structure resulting from the decay of excited states in xenon that lie between the $P_{1/2}$ and $P_{3/2}$ ionization continuum; electron energies from approximately 0.2 to 1.5 eV. Excitation of these states by proton impact leads to autoionization electrons that are observed superimposed on the continuum spectrum. The photoabsorption spectrum of xenon (Comes et al., 1968) for this energy range is also shown to illustrate which states contribute to the autoionization process. Also indicated in the figure are the positions of NOO Auger transitions that can be observed as small structures superimposed on the continuum spectrum for ejected electron energies between

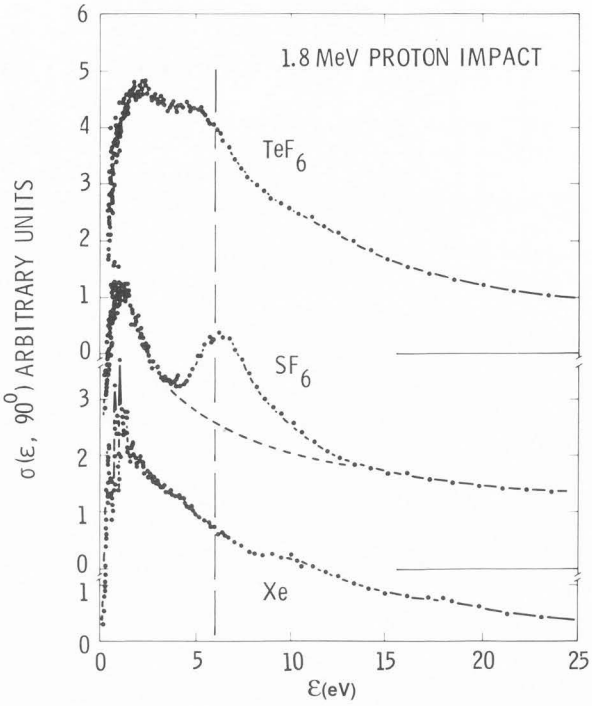


Fig. 11. Low-energy portion of spectra for ejection of electrons from $SF_6$, $TeF_6$ and Xe by 1.8-MeV protons. The data are from Toburen et al. (1977).

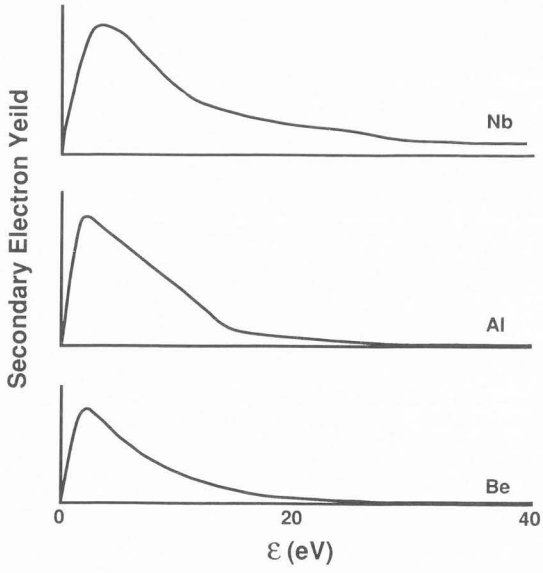


Fig. 12. Secondary electron yields induced by 0.5-MeV proton impact on clean metal surfaces. Data are from Hasselkamp et al. (1987).

about 8 and 40 eV. These result when N-shell vacancies are filled by an electron from the O-shell of xenon and the excess atomic energy is carried off by emission of an electron from the xenon O-shell.

Effects of molecular structure have also been observed in ejected electron spectra. Figure

11 shows data obtained in our laboratory for $SF_6$ and $TeF_6$ molecules (Toburen et al., 1977) compared with results obtained for the atomic xenon target. The peak at about 6.8 eV in the $SF_6$ spectrum was interpreted as resulting from excitation of $1t_{2u}$ and $4t_{1u}$ electrons to the $2t_{2g}$ state with subsequent autoionization to the ground state of the $SF_6^+$ ion.

Structures in the spectra of electrons ejected from foils by ion impact have also been attributed to excitation of specific states of the target. Data from Hasselkamp et al.(1987) for electron emission produced by 500-keV proton bombardment of aluminum, beryllium, and niobium foils are shown in Fig. 12. Although all the spectra show a maximum for ejected electron energies near 2 eV, the structure in the spectrum of aluminum at about 11 eV is attributed to the decay of volume plasmons and the structure observed at approximately 26 eV in the niobium spectrum results from NVV Auger decay.

## Models of Secondary Electron Spectra

Models of the spectrum of electrons ejected in proton collisions with atomic and molecular targets provide a basis for understanding the systematics of the broad range of data available, aid in testing reliability of measured values, and enable extrapolation to regions where measurements are lacking or infeasible. In addition, models are important tools for incorporating data into calculations of energy transport in an efficient manner. The large dynamic range of the singly differential cross sections can be minimized and modeling can be simplified if one represents the data as the ratio of measured cross section to the Rutherford cross section per target electron. This ratio has also been shown to be very useful in testing the consistency and reliability of experimental data for ionization of atomic and molecular targets by both, electron and proton impact; see, for example Kim and Inokuti (1973), Kim (1975), Kim and Noguchi (1975), Toburen et al. (1978), and Goruganthu et al. (1987).

The Rutherford cross section is based on the collision of a charged particle with a free electron and is given by the formula

$$\frac{d\sigma}{dE} = \frac{4\pi a_0^2}{T}\left(\frac{R}{E}\right)^2, \qquad (1)$$

where $a_0$ in the Bohr radius (0.529Å), R is the Rydberg energy (13.6 eV), E is the energy transferred to the ejected electron and T is given by

$$T = mv^2/2 \qquad (2)$$

with v the incident particle velocity and m the electron mass. For a bound electron, Eq. 1 must be modified to

$$\frac{d\sigma_i}{dE} = \frac{4\pi a_0^2 R^2}{T}\frac{N_i}{(\epsilon+I_i)^2}, \qquad (3)$$

where $\epsilon$ is the kinetic energy of the ejected electron, $N_i$ is the number and $I_i$ is the binding

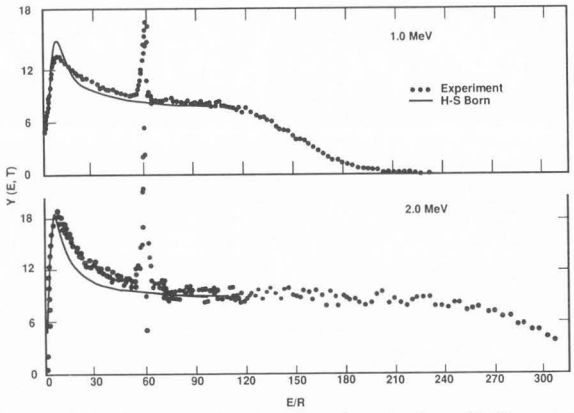


Fig. 13. Ratio of measured single differential cross sections for ionization of Ne by proton impact to the corresponding Rutherford values. Solid line is from a Born calculation described by Manson et al. (1975).

energy of electrons in the $i^{th}$ subshell. In most experiments there is no means of identifying the subshell of origin of the detected electrons, therefore the ionization potential in Eq. 3 is taken as the valence ionization potential which, at energies where the Rutherford formula is valid, is the primary contributor to the total cross section. The ratio of experimental-to-Rutherford cross section is then given by

$$Y(E,T) = \frac{T}{4\pi a_0^2 R^2}(\epsilon+I)^2\frac{d\sigma}{d\epsilon}, \qquad (4)$$

where I is the valence, or outer shell, electron binding energy and $\frac{d\sigma}{d\epsilon}$ is the measured single differential electron emission cross section. Since the Rutherford cross section is derived per target electron the ratio Y(E,T) should approach the number of electrons in the target for electrons ejected with sufficiently high energies for the Rutherford model to be valid. A more detailed discussion of Eq. 4 can be found in the paper by Toburen et al. (1978).

Data for 1-MeV and 2-MeV proton impact ionization of neon are shown plotted as the ratio of experimental-to-Rutherford cross sections in Fig. 13. For neon, as the ejected electron energy increases, Y(E,T) reaches a value approximately equal to the number of neon outer shell electrons, 8. This represents the expected behavior for a Rutherford collision between the proton and the "free" electrons in neon. The reduction in this ratio at the high-energy end of the spectrum reflects the maximum energy that can be transtransferred to a free electron in a binary collision for ionization by protons of the energies shown. At the low-energy end of the spectra, the ratio increases markedly above the Rutherford value. Low-energy electrons are ejected in "soft" collisions involving large impact parameters, with energy being transferred to the atom as a whole.

The theoretical cross sections shown as solid curves in Fig. 13 were obtained from a first Born calculation (Manson et al., 1975) using Hartree-Slater wave functions for both the initial discrete and final continuum states. The Born

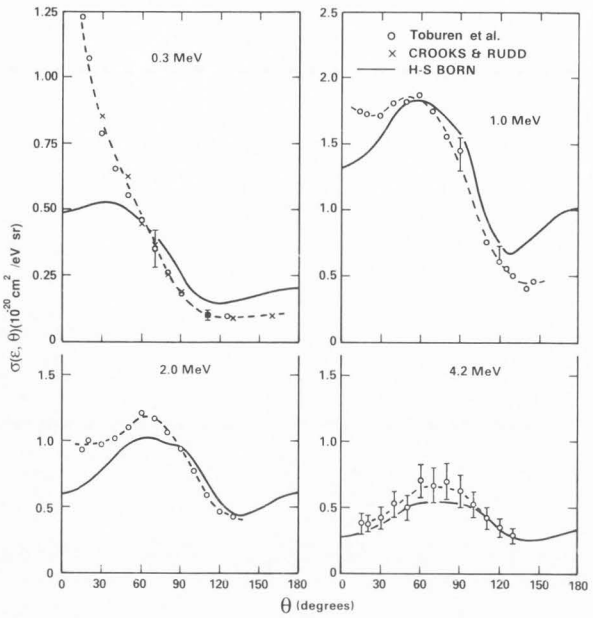


Fig. 14. Comparison of measured angular distribution for 81.6-eV electrons ejected from Ne by protons of different energies. Solid curves are from a Born calculation described by Manson et al. (1975). Experimental data are from (o) Toburen et al. (1978) and (x) Crooks and Rudd (1971).

calculation is in excellent agreement with the measured cross sections. Good agreement is also observed between Born results and measurements for the angular distributions of electrons ejected from neon by fast protons, shown in Fig. 14. These data are plotted on a linear scale which accentuates the differences between theory and experiment. In the angular distributions, the notable differences between theory and experiment occur for the low-energy proton impact and for electrons ejected into small angles. Cross sections in that region are strongly enhanced by the continuum-charge-transfer mechanism, which has not been included in the calculation. Although the Born theory provides accurate cross sections for ionization of neon, this computational method is limited to atomic targets by the unavailability of reliable wave functions describing more complex systems.

A very useful model of singly differential cross sections for electron ejection by proton impact has been developed by Miller et al., (1983). This model, based on Born theory, can readily be applied to molecular targets. Miller's model makes use of the Bethe expansion of the Born approximation in which the ionization cross section, differential with respect to energy loss, E, is given by

$$\frac{d\sigma}{dE} = \frac{4\pi a_0^2 Z^2}{T}\left[\frac{R^2}{E}\frac{df}{dE}\ln\left(\frac{4T}{R}\right) + B(E) + O\left(\frac{E}{T}\right)\right] \quad (5)$$

where $a_0$ is the Bohr radius, R is the Rydberg energy, $T = mv^2/2$ (m is the electron mass and v the ion velocity,) $E = \epsilon + I$ (I is the electron

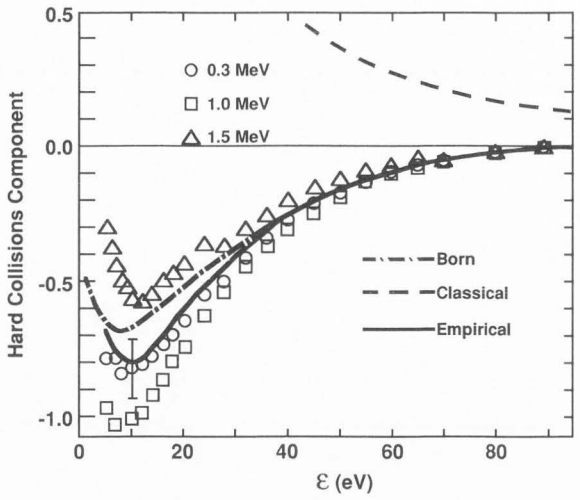


Fig. 15. Hard-collision component, B(E), of the Bethe expansion, obtained from experimental data for ionization of Ne by protons. Analysis described by Miller et al. (1983).

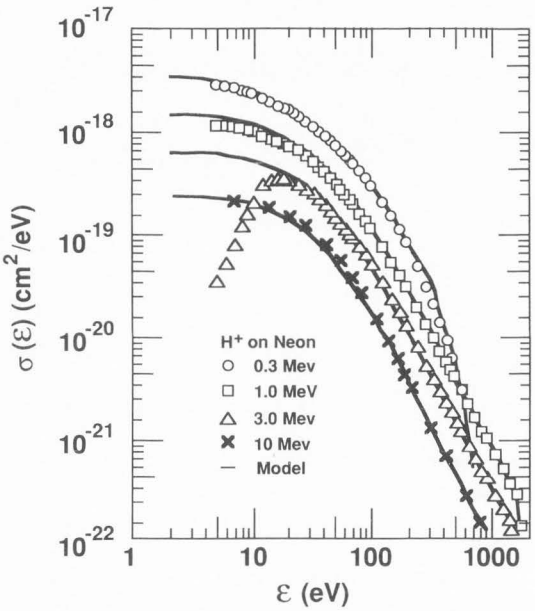


Fig. 16. Model calculations (solid lines) compared to experimental and theoretical single differential cross sections for electron emission from Ne by protons. Model and Born calculations are described by Miller et al. (1983).

binding energy and $\epsilon$ the secondary electron energy), and df/dE is the optical oscillator strength. This approximation conveniently separates the ejected electron spectrum into a soft-collision component proportional to df/dE and a hard-collision component B(E); O(E/T) in Eq. 5 includes terms of higher order in E/T and is considered negligible in this model. The high-energy behavior of the hard-collision part of the expression can be estimated from Rutherford or binary encounter theory, and the soft-collision part is provided by data from optical oscillator

strengths. The latter can be determined from photoabsorption data.

Equation 5 provides insight into the dependence of the differential cross section for electron production on incident ion energy. The soft collision component that results in emission of low-energy electrons varies with ion energy as lnT/T, whereas fast electrons ejected in hard collisions will decrease as 1/T. This model also illustrates that the target structure is predominantly reflected in the soft-collisions term. Because the low-energy end of the ejected electron spectra is dependent on the oscillator strength, we would expect variations in spectra from molecule to molecule (as was observed in Fig. 8) based on the difference in oscillator strengths observed for different molecules.

Unfortunately, the expression presented as Eq. 5 is not readily usable as an ab initio method for calculation of cross sections for complex targets because theoretical evaluation of B(E) involves computation with wave functions of the collision system. The model of Miller et al. (1983) overcomes this limitation by using experimental data data for $\frac{d\sigma}{dE}$ and $\frac{df}{dE}$ to evaluate B(E). Note that B(E) is independent of proton energy. Thus, if data are available at any proton energy for determination of B(E), the model can be applied at any other energy for which the Born theory is valid.

The hard-collision component B(E), evaluated for neon for three different proton energies, is shown in Fig. 15. The variation of B(E) with proton energy observed in Fig. 15 is attributed to uncertainties in the experimental data. The empirical curve was, therefore, drawn through the average of the experimental values. The results of classical binary encounter theory are also shown in Fig. 15. Classical theory grossly overestimates the low-energy end of the hard-collision spectrum. Using the empirical hard-collisions spectrum obtained from the data shown in Fig. 15, model calculations of the singly differential cross sections for proton impact ionization of neon were performed, and the results are compared with measured and ab initio calculations in Fig. 16. The agreement observed with measurements for 0.3-MeV and 1.0-MeV protons confirms the consistency of the fit to obtain model parameters. The model calculation for 3-MeV protons agrees well with measurements from our laboratory for electron energies greater than about 20 eV. In this case the measurements were performed with electrostatic electron energy analysis in which low-energy transmission was poor, i.e., data below about 20 eV are unreliable. This comparison with the 3-MeV data illustrates the power of the model in providing reliable data where direct measurements are lacking. The model calculations are also in excellent agreement with a full Born calculation conducted for 10-MeV protons. This model has also been applied to a number of simple molecular targets with equally good results (Wilson et al.(1984)). An additional strength of this model is that since the target dependence is given primarily by the optical oscillator strength, the model can provide single differential cross sections for electron production in condensed-phase targets merely by using the proper target oscillator strengths. In many cases, oscillator strengths are available, or can readily be obtained, where direct measurements of differential ionization spectra are infeasible.

The model described above can be a valuable tool for calculating cross sections for different materials where only sparse data are available, although its use is limited to the ion velocity range of validity of the Born approximation. Recently, Rudd (1988) has published a model that can be used to provide cross sections over the complete range of proton energies. He presents an analytical expression developed by combining features of the binary encounter theory, the Bethe approximation, and the molecular promotion model. Adjustable parameters of the model are determined by fitting the available single differential cross sections. The advantage of this model is that once the parameters have been determined, the model can be used to predict cross sections over a wide range of proton energies, even to very low energies that are not accessible to the Miller model. On the other hand, disadvantages of this model are that it requires a fairly extensive set of data to determine the model parameters and, in principle, they must be determined independently for each projectile-target system. Thus, model parameters determined for one set of collision partners are not directly applicable to another collision system. However, many of the parameters are relatively independent of the target, and others are sufficiently well behaved that good guesses can be made for parameters, enabling reasonable estimates of differential cross sections where no data exist.

The analytical expression developed by Rudd can be written in the following form:

$$\sigma(\epsilon) = \frac{4\pi a_0^2 N R^2 [F_1(v)+\epsilon F_2(v)]}{I^3(1+\epsilon)^3\{1+\exp[\alpha(\epsilon-\epsilon_c)/v]\}}, \qquad (6)$$

where $a_0$ is the Bohr radius, N is the number of target electrons with binding energy I, R is the Rydberg unit of energy (R = 13.6eV), v is the reduced ion velocity [$v = (T/I)^{1/2}$, T = mE/M (E is the ion energy, M is the ion mass, m is the electron mass)], $\epsilon_c$ is a cut-off energy ($\epsilon_c = 4v^2 - 2v - R/4I$), and $\alpha$, $F_1(v)$, and $F_2(v)$ are fitting parameters. The parameter $\alpha$ varies only slightly over the entire energy range and is taken as a constant for a given target. The functions $F_1(v)$ and $F_2(v)$ are nearly independent of velocity at low ion energies, but show a decrease with increasing ion energy in the high energy region. The velocity dependence of these functions can also be fitted, maintaining the separability of high and low energy behavior, with the following equations

$$F_1 = L_1+H_1, \qquad (7)$$

and

$$F_2 = L_2H_2/(L_2+H_2), \qquad (8)$$

where

$$H_1 = A_1 \ln(1+v^2)/(v^2+B_1/v^2), \qquad (9)$$

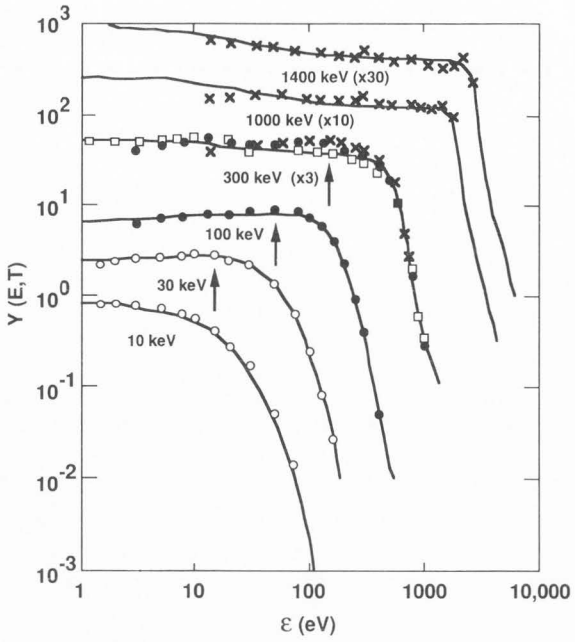


Fig. 17. Comparison of results obtained from model of Rudd (1988) with measured values of single differential cross sections for ejection of electrons from molecular nitrogen by protons of various energies. Experimental data are from (o) Rudd (1979), (●) Crooks and Rudd (1971), (x) Toburen (1971), and (□) Stolterfoht (1971). The arrows indicate the position for ejected electrons of the same velocity as the incident proton.

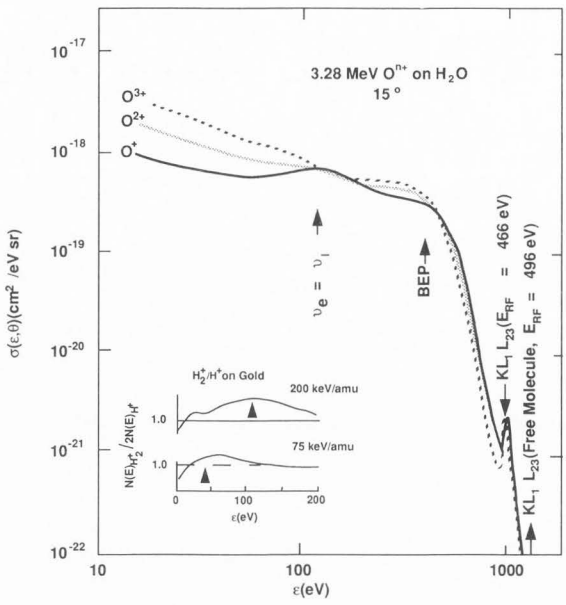


Fig. 18. Spectrum of electrons ejected at 15° from water vapor by 3.28-MeV oxygen ions of various charge states. Insert shows ratio of yields of electrons ejected from a gold target by equal-velocity $H^+$ and $H_2^+$ ions (Hasselkamp et al., 1984).

$$H_2 = A_2/v^2+B_2/v^4, \tag{10}$$

$$L_1 = C_1 v^{D1}/(1+E_1 v^{(D_1+4)}), \tag{11}$$

and

$$L_2 = C_2 v^{D_2}. \tag{12}$$

The parameters, $A_1,\ldots, E_1$ and $A_2,\ldots, D_2$ plus $\alpha$ then become the 10 basic fitting parameters for each electronic shell of each target. These parameters have been published for proton ionization of $H_2$, He, and Ar (Rudd, 1988) and He, Ne, Ar, and Kr (Cheng, et al., 1989). Data for $N_2$, $CO_2$, $H_2O$, and $O_2$ are available from Rudd (Private Communication, 1989).

The model of Rudd reduces to that of Miller, discussed above, in the limit of high energy proton impact. At high ion velocities the exponential term in Eq. 6 approaches a constant, and the ion velocity dependence expressed by $F_1(v)$ and $F_2(v)$ corresponds to, respectively, the soft- and hard-collision characteristics discussed above for the Miller model. On the other hand, for small ion velocities, the exponential term will dominate. In that case, the differential cross section will increase with increasing ion energy, approximately as $T^{1/2}$, reflecting the relationship between $\epsilon_c$ and the ion energy. For a given low-velocity ion, the ejected electron energy spectrum will exhibit an exponential decrease with increasing electron energy.

An example of the consistency in fitting data for a wide range of proton energies where this model is applied to proton impact ionization of molecular nitrogen (Rudd, Private Communication) is shown in Fig. 17. In fitting the nitrogen data, Rudd used the following sets of model parameters: for the outer shell $A_1 = 1.05$, $B_1 = 12.0$, $C_1 = 0.74$, $D_1 = -0.39$, $E_1 = 0.80$, $A_2 = 0.95$, $B_2 = 1.20$, $C_2 = 1.00$, $D_2 = 1.30$ and $\alpha = 0.7$; and for the inner shell $A_1 = 1.25$, $B_1 = 0.50$, $C_1 = 1.00$, $D_1 = 1.00$, $E_1 = 3.0$, $A_2 = 1.10$, $B_2 = 1.30$, $C_2 = 1.00$, $D_2 = 0.00$ and $\alpha = 0.66$. With these parameters the model, shown as the solid line in the figure, provides a consistent fit throughout the entire proton energy range. The arrows in Fig. 17 indicate the position where one would expect the maximum contributions from continuum charge transfer. Although this model does not incorporate explicit features of continuum charge transfer, the fit to experimental data in this region is excellent. One of the applications of such a model is to test the consistency of experimental data. For instance, if any of the data from Rudd (1979), Crooks and Rudd (1971), Toburen (1971) or Stolterfoht (1971) that are shown in Fig. 17 differed markedly from the model predictions, one would be justified in questioning the reliability of those data. Fortunately data from the different laboratories are in excellent agreement with each other and with the model prediction.

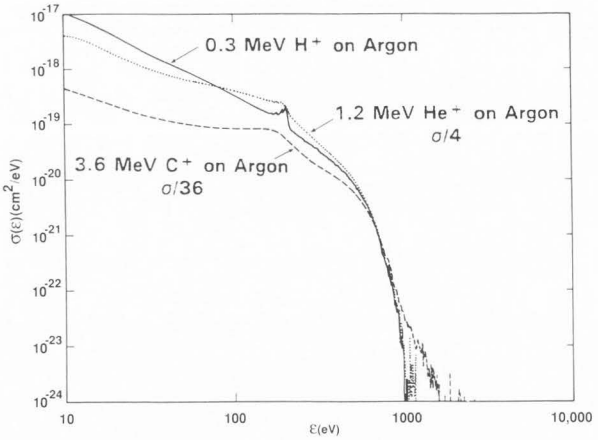


Fig. 19. Comparison of spectra for electrons ejected from argon by different ions. For comparison, cross sections have been divided by the square of their respective nuclear charges.

## Interactions of Structured Ions with Atoms and Molecules

Although there are a great deal of data and a relatively good theoretical understanding for ionizing collisions involving bare charged particles and atomic and molecular targets, very little is known regarding interactions involving ions that carry bound electrons. These ions, referred to as "clothed" or "structured" ions, lose energy through interactions involving a screened nuclear, or effective ionic charge. The features observed in the spectrum of electrons ejected in single collisions of oxygen ions of different charge states with water vapor are illustrated in Fig. 18 for ejection of electrons at 15° with respect to the beam direction. In addition to the spectral features noted earlier for bare ion impact, a prominent peak is observed at an electron energy corresponding to that of electrons with the same velocity as the ion and a new peak is observed superimposed on the continuum at the extreme high-energy end of the spectrum. The peak at the upper end of the spectrum results from Auger electrons emitted in the rest frame of the moving ion that are then observed at a Doppler-shifted energy in the laboratory frame of reference. The energy of the Doppler-shifted projectile Auger peak is observed at a somewhat lower energy than that calculated for a moving oxygen atom, the calculated atomic value is shown in Fig. 18 as the arrow labeled "free molecule." This energy shift is attributed to involvement of the more tightly bound electrons of the ion in the energetics of the Auger process. The equal-velocity peak, labeled $v_e = v_i$, results from electrons being stripped from the moving oxygen ion. The relative size of this contribution decreases with increasing charge state of the ion, reflecting the smaller number of bound electrons available to be stripped from the ion. Although continuum charge transfer would also be expected to contribute to the spectrum in this region, its contribution is negligible compared to that from electron loss from the projectile.

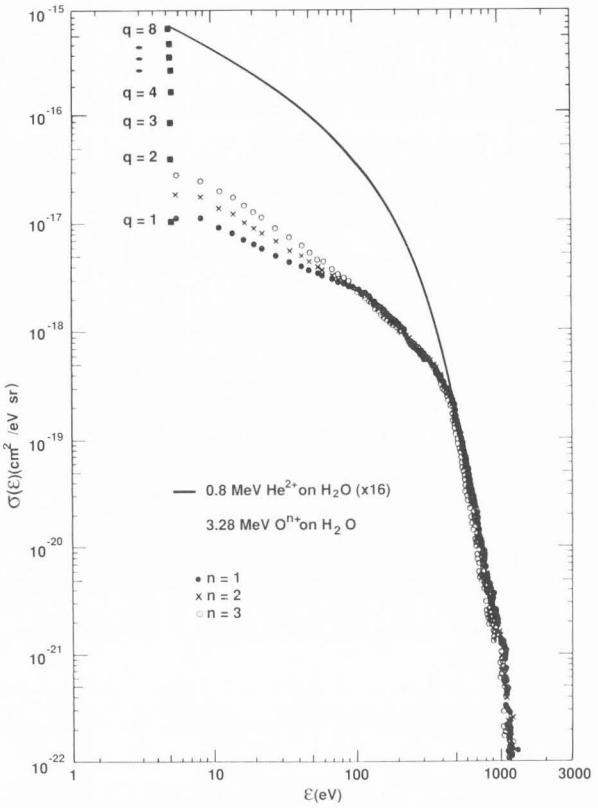


Fig. 20. Comparison of spectra of electrons ejected from water vapor by oxygen ions with those produced by $He^{2+}$ impact. Results for $He^{2+}$ have been scaled to oxygen by multiplying $He^{2+}$ cross sections by square of ratio of oxygen-to-helium nuclear charge.

The effect of projectile electrons in screening the ion nucleus is evident in Fig. 18 as the reduction in the relative magnitude of the cross sections for emission of low-energy electrons as the number of bound projectile electrons increases. The ejection of low-energy electrons occurs with large-impact parameters where the projectile electrons provide an effective electrostatic shield of the ion nucleus. Fast electrons, on the other hand, are emitted from close collisions that take place within the spatial distribution of charge presented by the projectile elections. The latter is reflected in Fig. 18 where, as the ejected energy increases, all three ion charge states are nearly equal in their ionization efficiency.

The screening effect of projectile electrons as well as the loss of electrons from the ion have also been observed in electrons ejected from solid targets. See, for example, the data for electrons ejected from gold foils by $H_2^+$ ions (Hasselkamp et al., 1984), illustrated in the lower-left portion of Fig. 18. This insert shows the Hasselkamp data for two sets of ion velocities plotted as the ratio of secondary electron yields for $H_2^+$ impact to twice the yield for equal-velocity $H^+$ impact. The ratio becomes less than 1 for small electron energies, reflecting the screening of the $H_2^+$ ion charge by the bound

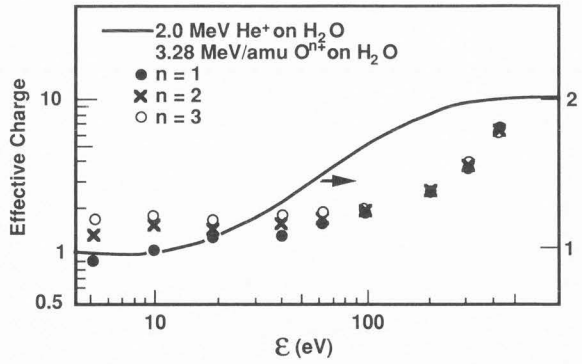


Fig. 21. Observed effective nuclear charge as a function of energy loss for ionization by $O^{n+}$ and $He^+$ ions. For $He^+$ data use scale to right.

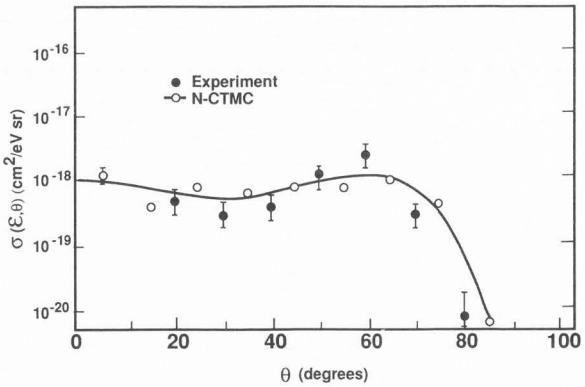


Fig. 22. Cross sections for ejection of 500-eV electrons from argon by 1.4-MeV/amu $U^{33+}$ ions; experiment and theory. Data described by Schmidt et al. (1989). Theory is a classical trajectory Monte Carlo calculation of Schmidt et al. (1989).

projectile electron. The ratio becomes greater than 1 for ejected electron velocities near the ion velocity owing to electron loss from the projectile in a manner quite similar to that observed in the gas-phase data. This increase is attributed to the electron from the $H_2^+$ ion being stripped from the ion and elastically backscattered from the foil.

If we compare ejected electron spectra for different ions for the same target and the same ion velocity, it is possible to investigate the effects of electron screening on the cross section for electron production and thus for energy loss. Such a comparison is shown in Fig. 19 for the spectra of electrons ejected from argon by $H^+$, $He^+$ and $C^+$ ions; in each case the cross sections have been divided by the square of the nuclear charge of the projectile to provide a basis for comparison. Compared in this way, the cross sections for ejection of the high-energy electrons by the different ions are in good agreement. The implication of this agreement is that the impact parameters associated with high-energy losses are sufficiently small that the projectile electrons are inefficient in screening the nuclear charge. On the other hand, for small energy transfer, large-impact parameters are involved, and the projectile is appropriately screened by its bound electrons, leading to large differences in the low-energy electron yields for these ions when scaled in this manner.

A more quantitative estimate of the effects of screening by projectile electrons can be obtained from the data shown in Fig. 20; here, cross sections for electron ejection from water vapor by oxygen ions with charge states 1-3 are compared with similar data for bare ion ($He^{2+}$) impact (Toburen et al., 1980). The $He^{2+}$ data have been scaled by $Z^2$ to represent a bare charge of Z = 8 for comparison to the oxygen ion results. This comparison illustrates the large decrease in the cross section for ejection of low-energy electrons from the target molecule by the screened oxygen ions relative to that expected for a bare charge, as predicted by the scaled $He^{2+}$ data. For sufficiently distant collisions, i.e., small energy transfer, we would expect the oxygen ion to interact like a point charge of magnitude equal to its net charge q, where q is given by Z - ne with n the number of bound projectile electrons and e the electronic charge. For these distant collisions the ionization cross section would then be expected to scale as $q^2$ rather than $Z^2$. The square points plotted at $\epsilon$ = 5 eV in Fig. 20 show the expected $q^2$ dependences for low-energy electrons ejected by ions with charge states from q = 1 to q = 8. The disagreement between the expected low-energy behavior and that measured for q = 1-3 indicates that the 5-eV data shown in Fig. 20 are not of sufficiently low energy for this expectation to be reached or that other ionization mechanisms, not scaling as $q^2$, are dominating the emission of low energy electrons.

It is possible to determine an effective charge of the incident ion as a function of energy loss by comparing the cross sections for clothed ions with similar data for a bare ion. The effective charge determined for the oxygen ion data of Fig. 20 with reference to bare $He^{2+}$ cross sections is shown in Fig. 21. Also shown in Fig. 21 are data for the effective charge of $He^+$ ions as discussed by Toburen et al. (1981 a,b); the right hand scale applies to the $He^+$ data. These data clearly indicate that the effective nuclear charge depends not only on the energy of the ejected electron, but also on the type of ion. We may also expect that the effective charge will depend on the energy of the ion and on the electronic structure of the target, although this has not been explicitly shown.

The primary reason for discussing the differential cross sections for clothed ions is to point out the difficulty associated with application of an effective charge concept outside of its original definition in stopping-power theory. With regard to interactions of ions leading to secondary electron emission, or energy loss, there is often confusion over the use of the concepts of effective charge, net ion charge, and equilibrium charge. Certainly, equilibrium charge and net ion charge have little correlation with energy loss and electron production. Likewise, the effective charge of stopping-power theory will not be useful in estimating the differential cross sections for electrons liberated in interactions with ions.

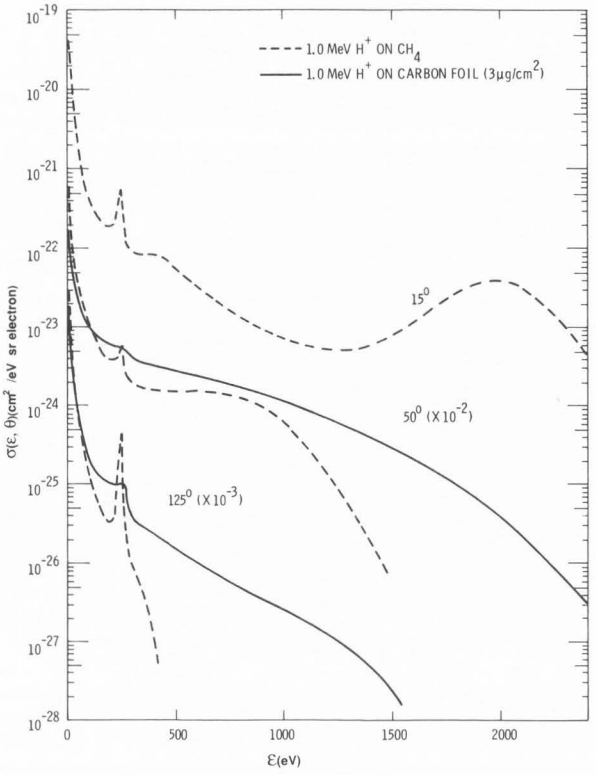


Fig. 23. Comparison of doubly differential cross sections for ejection of electrons from methane gas and from 3-$\mu$g/cm$^2$ carbon foil by 1-MeV protons.

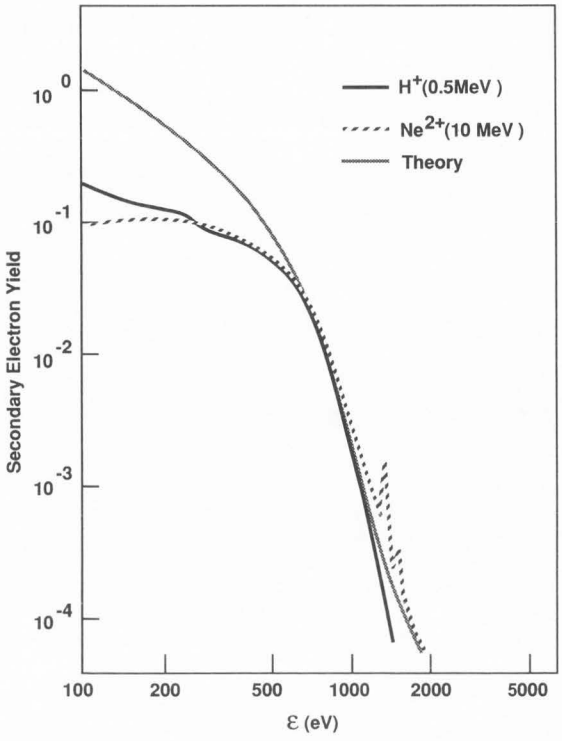


Fig. 24. Secondary electron distributions observed at 42.3° from a 20-$\mu$g/cm$^2$ carbon foil produced by 0.5-MeV/amu $H^+$ and $Ne^{2+}$ ions. Theoretical data, based on a binary encounter approximation, and experimental data have been normalized together at electron energy of approximately 800 eV. Data are from Folkmann et al. (1975).

What is more appropriate to differential cross sections is an effective charge that is defined as a function of energy, or momentum, transfer. At the present time, however, there does not appear to be a theoretical or experimental description that is appropriate for quantitatively describing interactions involving clothed ions, even for atomic targets. Born theory can provide a framework for simple atomic systems, but even for these systems the results are preliminary and largely untested (McGuire et al., 1981), (Manson and Toburen, 1981). New hope in our ability to better understand heavy-ion collisions may be generated by the recent increase in activity in the study of ionization at high energies (Schmidt et al., 1989), (Stolterfoht et al., 1987). Doubly differential cross sections from the work of Schmidt et al. are shown in Fig. 22, where the angular distribution of 500-eV electrons ejected in collisions of 1.4-MeV/amu $U^{33+}$ ions with argon are compared with a recent calculation by the classical-trajectory-Monte-Carlo (CTMC) method. The excellent agreement between theory and experiment in these high-energy collisions should encourage investigators to apply similar techniques to lower-energy systems involving light ions.

## Electron Emission from Foils

Very few data are available regarding absolute cross sections, differential in energy and angle, for electrons ejected from thin foils by ions. Difficulties in maintaining foil cleanliness and uncertainties in foil thickness have, in many cases, precluded determination of reliable absolute values. An indication of the differences in spectra recorded for solid and gas targets is illustrated in Fig. 23, where spectra for electrons ejected from a 3-$\mu$g/cm$^2$ carbon foil and from methane gas are shown. The foil measurements were made in our laboratory with the apparatus shown in Fig. 1. We simply removed the gas target cell and installed a foil holder to make measurements for the carbon foil. The Faraday cup also had to be relocated for the foil measurements because it was an integral part of the target cell. Relocating the Faraday cup to the wall of the vacuum chamber reduced the angular range we could investigate to angles from 50° to 125°. With these minor modifications, the system has the advantage of providing good comparisons of gas versus foil data, but the disadvantage that our vacuum system ($10^{-6}$ Torr), designed for gas targets, was not sufficient to maintain a clean foil target. Lack of foil cleanliness, along with uncertainty in foil thickness, prevented us from having confidence in the absolute cross section values, although we estimate that they may be accurate to a factor of 2. Nevertheless, the comparison of foil and gas data in Fig. 23 shows qualitatively what might be expected. The cross sections per loosely bound

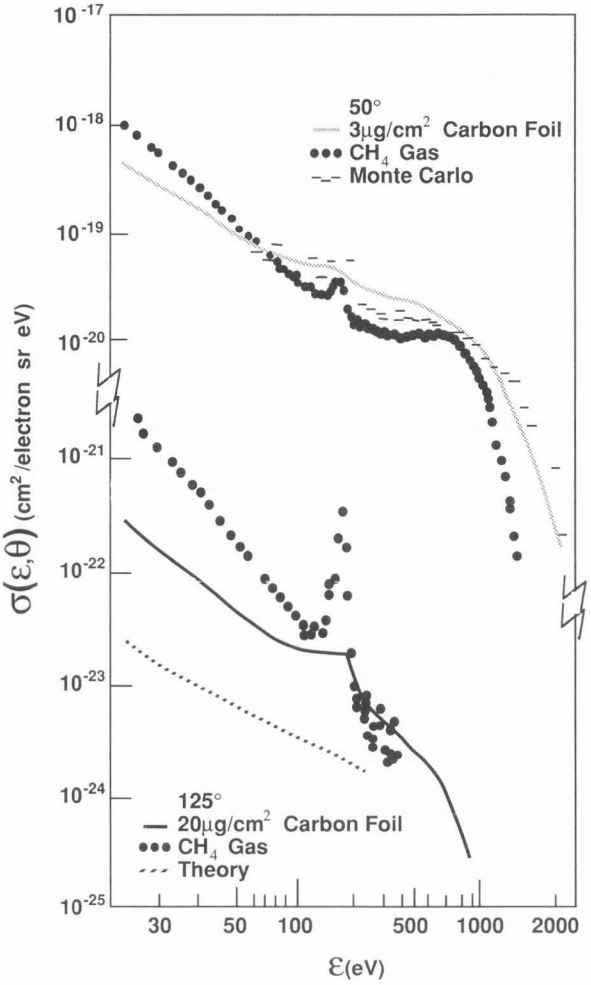


Fig. 25. Upper part: Comparison of measurements of cross sections for electrons ejected at 50° from 3-$\mu$g/cm2 carbon foil by 1-MeV protons with those emitted from $CH_4$ gas. Also shown are Monte Carlo calculations for electron emission from foil normalized to measurements at approximately 100 eV. Lower portion: Data for electron emission at 125° by 1-MeV proton impact on CH4 gas and 20-$\mu$g/cm2 carbon foil compared with the foil calculation of Schou (1980). Electron spectra and Monte Carlo calculations from carbon foils described by Wilson et al. (1978).

target electron for ejection of low-energy electrons from the foil are somewhat smaller than the comparable values for the gas target. This is reasonable, because the low-energy electrons are strongly absorbed in the foil. At higher energies, the cross sections for ejection of electrons from the foil are greater than those from the gas. This is also predictable because higher-energy electrons originally produced within the foil with small emission angles can be scattered and detected in the spectra described at larger angles.

Figure 24 shows secondary electron yields published by Folkmann et al. (1975) for electrons ejected at 42.3° with respect to 0.5-MeV/amu beams

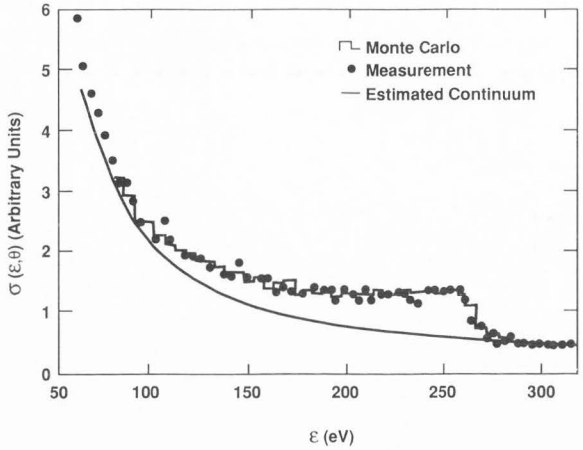


Fig. 26. Comparison of measured and calculated shape of carbon K-Auger electron spectrum emitted at 50° from 1-MeV proton bombardment of 3-$\mu$g/cm$^2$ carbon foil. Monte Carlo results normalized to measurements at 250 eV. Data described in the Toburen et al. (1982).

of $H^+$ and $Ne^{2+}$ ions through a 20-$\mu$g/cm$^2$ carbon foil. These spectra were reported as relative values and have been renormalized in this figure so that the proton- and neon-induced spectra agree at approximately 800 eV. This renormalization is consistent with the way heavy-ion cross sections were found to scale for gases (see Fig. 20) and is reasonably consistent with the observation of these authors that the total electron yields were in approximately the ratio of the square of the nuclear charge of the two projectiles. The theoretical curve presented in Fig. 24 was calculated by Folkmann et al. (1975) based on a binary encounter approximation for the initial electron production and subsequent electron slowing down based on Bethe stopping theory. Although good agreement is obtained with the measured spectra for high-energy ejected electrons the model grossly overestimates the low-energy portion of the spectra.

Two additional features of the data shown in Fig. 24 are worth noting. First, after the renormalization of the $Ne^{2+}$ data to coincide with the high-energy proton data, we can see evidence of electronic screening of the neon nucleus in the production of low-energy electrons. Further evidence for electronic structure of the neon ion can be seen in the peaks superimposed on the high energy tail of the ejected electron spectrum. Such peaks are the result of inner shell vacancies produced in the K-shell of neon being filled by Auger processes involving electrons in the outer shells of neon. Careful analysis of these peak energies and intensities could provide detailed information on the charge state of the neon ion when it exits the foil.

Calculations of electron production and their subsequent degradation from ions passing through foils have been undertaken by analytic methods (Schou, 1980) and by Monte Carlo techniques (Wilson et al., 1978). The upper portion of Fig. 25 shows data from our laboratory for electron emission at 50° with respect to 1-MeV protons

passing through a 3-$\mu$g/cm2 carbon foil and from methane gas compared to the Monte Carlo calculation of Wilson et al. (1978). Agreement in spectral shape between the calculation and foil measurement is excellent. In the lower portion of the figure, the theoretical results of Schou (1980) are compared to our measurements for electrons emitted from a 20-$\mu$g/cm$^2$ carbon foil at 125° with respect to a 1-MeV proton. Although the general shape of the calculated spectrum is in agreement with the measured spectrum, the absolute magnitudes of the two sets of data differ by a factor of about 5.

The shape of the Auger electron distribution determined by Monte Carlo electron transport following 1-MeV proton excitation of a 3-$\mu$g/cm2 carbon foil (Toburen et al., 1982) is compared to the measured spectrum in Fig. 26. The calculated and measured spectra are normalized together at 250 eV. Excellent agreement with the shape of the Auger spectrum is obtained with the calculation. However, the absolute magnitude of the cross sections again differ; in this case, the measured values are a factor of approximately 3 larger then the Monte Carlo result.

Although we understand many of the basic features observed in the spectrum of electrons ejected from foils by ions we still lack a quantitative theory of the electron emission process. With renewed interest in studies of the energy and angular distributions of electrons from foils, greater emphasis on high-vacuum techniques, and application of recent advances in computational techniques, there should be a great deal of progress in understanding these processes in the coming years.

## Acknowledgements

Work supported by the Office of Health and Environmental Research (OHER), U.S. Department of Energy under Contract DE-AC06-76RLO 1830.

## References

Berenyi D. (1987). Present experimental approach and some recent measurements in ion-atom collision research, Vacuum 37, 53-59.

Breinig M, Elston SB, Huldt S, Liljeby L, Vane CR, Berry SD, Glass GA, Schauer M, Sellin IA, Alton GD, Datz S, Overbury S, Laubert R, Suter M. (1982). Experiments concerning electron capture and loss to the continuum and convoy electron production by highly ionized projectiles in the 0.7- to 8.5-MeV/amu range traversing the rare gases, polycrystalline solids, and axial channels in gold, Phys. Rev. A 25, 3015-3378.

Cheng W, Rudd ME, Hsu Y. (1989). Differential cross sections for ejection of electrons from rare gases by 75-140 keV protons, Phys. Rev. A 39, 2359-2366.

Comes FJ, Salzer HG, Schumpe G. (1968). Autoionisation in atomspektren, Z. fur Naturforsch. 23, 137-151.

Criswell TL, Toburen LH, Rudd ME. (1977). Energy and angular distribution of electrons ejected from argon by 5-keV to 1.5-MeV protons, Phys. Rev. A 16, 508-517.

Crooks GB, Rudd ME. (1970). Experimental evidence for the mechanism of charge transfer into continuum states, Phys. Rev. Lett. 25, 1599-1601.

Crooks JB, Rudd ME. (1971). Angular and energy distribution of cross sections for electron production by 50-300-keV proton impact on $N_2$, $O_2$, Ne, and Ar, Phys. Rev. A 3, 1628-1634.

Focke P, Nemirovsky IB, Lepera EG, Meckbach W. (1984). Beam-foil convoy electron distributions as a function of energy and angle of emission, Nucl. Instrum. Meth. B2, 235-240.

Folkmann F, Groeneveld KO, Mann R, Nolte G, Schumann S, Spohr R. (1975). Continuous electron energy spectra ejected from solid carbon targets bombarded with light and heavy ions, Z. Phy. A 275, 229-233.

Gabler H. (1974). Emission von elektronen beim stoss hochenergetischer protonen mit argon, Diplom thesis, Freie Universitat Berlin.

Goruganthu RR, Wilson WG, Bonham RA. (1987). Secondary-electron production cross sections for electron-impact ionization of molecular nitrogen, Phys. Rev. A 35, 540-558.

Hasselkamp D, Hippler S, Scharmann A. (1984). Molecular effects in the energy spectrum of ion-induced secondary electrons from gold, Nucl. Instrum. Meth. B2, 475-478.

Hasselkamp D, Hippler S, Scharmann A. (1987). Ion-induced secondary electron spectra from clean metal surfaces, Nucl. Instrum. Meth. B18, 561-565.

Kennedy DJ, Manson ST. (1972). Photoionization of the noble gases: Cross sections and angular distributions, Chem. Phys. Lett. 30, 227-247.

Kim Y-K. (1975). Energy distribution of secondary electrons I. Consistency of experimental data, Radiat. Res. 61, 21-35.

Kim Y-K, Inokuti M. (1973). Slow electrons ejected from He by fast charged particles, Phys. Rev. A 7, 1257-1260.

Kim Y-K, Naguchi T. (1975). Secondary electrons ejected from He by protons and electrons. Int. J. Radiat. Phys. Chem. 7, 77-82.

Latz R, Schader J, Frischkorn HF, Hofman D, Koschar P, Groeneveld KO. (1984). The relation between convey electron velocity and ion velocity of ions penetrating solids, Nucl. Instrum. Meth. B2, 245-247.

Lynch DJ, Toburen LH, Wilson WE. (1976). Electron emission from methane, ammonia, monomethylamine, and dimethylamine by 0.25 to 2.0 MeV protons, J. Chem. Phys. 64, 2616-2622.

Manson ST, Toburen LH. (1981). Energy and angular distributions of electrons from fast $He^+$ + He collisions, Phys. Rev. Lett. 46, 529-531.

Manson ST, Toburen LH, Madison DH, Stolterfoht N. (1975). Energy and angular distribution of electrons ejected from helium by fast protons and electrons: theory and experiment, Phys. Rev. A 12, 60-79.

McDaniel EW, Flannery MR, Thomas EW, Ellis HW, McCann KJ, Manson ST, Gallagher JW, Ruble JR,

Beaty EC, Roberts TG. (1979). Compilation of data relevant to nuclear pumped lasers, US Army Missile Research and Development Command Technical Report H-78-1, Vol. V, Redstone Arsenal, Alabama, 2295-2375.

McGuire JH, Stolterfoht S, Simony PR. (1981). Screening and antiscreening by projectile electrons in high-velocity atomic collisions, Phys. Rev. A 24, 97-102.

Meckbach W, Focke PJ, Goni AR, Suarez S. (1986). Effects of the Wannier ridge on secondary-electron spectra in proton-helium collisions, Phys. Rev. Lett. 57, 1584-1590.

Miller JH, Toburen LH, Manson ST. (1983). Differential cross sections for ionization of helium, neon, and argon by high-velocity ions, Phys. Rev. A 27, 1337-1344.

Neelavathi VN, Ritchie RH, Brandt W. (1974). Bound electron states in the wake of swift ions in solids, Phys. Rev. Lett. 33, 302-305.

Ogurtsov GN. (1972). Energy spectrum of electrons ejected in ion-atom collisions. Rev. Mod. Phys. 44, 1-17.

Rudd ME. (1975). Mechanisms of electron production in ion-atom collisions, Radiat. Res. 64, 153-180.

Rudd ME. (1979). Energy and angular distributions of electrons from 5-100-keV-proton collisions with hydrogen and nitrogen molecules, Phys. Rev. A 20, 787-796.

Rudd ME. (1988). Differential cross sections for secondary electron production by proton impact, Phys. Rev. A 38, 6129-6137.

Rudd ME, Jorgensen T. (1963). Energy and angular distribution of electrons ejected from hydrogen and helium by protons, Phys. Rev. 131, 666-675.

Rudd ME, Toburen LH, Stolterfoht N. (1979). Differential cross sections for ejection of electrons from argon by protons, Atomic Data and Nuclear Data Tables 23, 405-442.

Schader J, Latz R, Burkhard H, Frischkorn HJ, Hofman D, Koschar P, Groeneveld KO, Berényi D, Köver A, Szabo G. (1984). Target ionization and projectile electron loss in simple collision systems, J. Physique Lett. 45, 249-254.

Schmidt S, Euler J, Kelbch C, Kelbch S, Koch R, Kraft G, Olsen RE, Ramm U, Ullrich J, Schmidt-Böcking H. (1989). Double differential stopping powers of 1.4 MeV/amu $U^{33+}$ in Ne and Ar derived from electron production and multiple ionization cross sections, Report number GSI-89-19, Gesellschaft für Schwerionenforschung, D-6100 Darmstadt 11, West Germany.

Schou J. (1980). Transport theory for kinetic emission of secondary electrons from solids, Phys. Rev. B 22, 2141-2174.

Schou J. (1988). Secondary electron emission from solids by electron and proton bombardment, Scanning Microsc. 2, 607-632.

Siegbahn K, Nordling C, Johansson G, Hedman J, Hedén PF, Kamrin K, Gelius U, Bergmark T, Werme LO, Manne R, Baer Y. (1969). Auger electron spectra of the noble gases, in ESCA applied to free molecules, North Holland Publishing Co, Amsterdam, 156-163.

Stolterfoht N. (1971). Angular and energy distributions of electrons produced by 200-500 keV protons in gases: I. experimental arrangement. Z. Phys. 248, 81-93.

Stolterfoht N. (1978). Excitation in energetic ion-atom collisions accompanied by electron emission, In: Topics in Current Physics, Vol.5 (Sellin IA, ed.), Springer-Verlag, New York, 155-199.

Stolterfoht N. (1987). High resolution Auger spectroscopy in energetic ion atom collisions. Physics Reports 146, 315-424.

Stolterfoht N, Schneider D, Tanis J, Altevogt H, Salin A, Fainstein PD, Rivarola R, Grandin JP, Scheurer JN, Andriamonje S, Bertault D, Chemin JF. (1987). Evidence for two-center effects in the electron emission from 25 MeV/amu $Mo^{40+}$ +He collisions: Theory and experiment, Europhys. Lett. 4, 899-904.

Toburen LH. (1971). Distributions in energy and angle of electrons ejected from molecular nitrogen by 0.3-1.7 MeV protons. Phys. Rev. A 3, 216-227.

Toburen LH. (1982). Continuum electron emission in heavy ion-atom collisions, In: Nuclear Methods Monograph Series Vol.2 (Berenyi D, Hock G, eds.), Elsevier, New York, 53-82.

Toburen LH, Manson ST. (1975). Effects of the Cooper minimum on charged particle ionization, Chem. Phys. Lett. 30, 114-115.

Toburen LH, Wilson WE. (1975). Time-of-flight measurements of low-energy electron energy distributions from ion-atom collisions, Rev. Sci. Instrum. 46,851-854.

Toburen LH, Wilson WE. (1977). Energy and angular distributions of electrons ejected from water vapor by 0.3-1.5 MeV protons, J. Chem. Phys. 66, 5202-5213.

Toburen LH, Wilson WE, Porter LE. (1977). Energy and angular distributions of electrons ejected in the ionization of $SF_6$ and $TeF_6$ by fast protons, J. Chem. Phys. 67,4212-4221.

Toburen LH, Manson ST, Kim Y-K. (1978). Energy distributions of secondary electrons. III. Projecticle energy dependence for ionization of He, Ne, and Argon by protons, Phys. Rev. A 17, 148-159.

Toburen LH, Wilson WE, Popowich RJ. (1980). Secondary electron emission from ionization of water vapor by 0.3- to 2.0-MeV $He^+$ and $He^{2+}$ ions, Radiat. Res. 82, 27-44.

Toburen LH, Stolterfoht N, Ziem P, Schneider D. (1981a). Electronic screening in heavy ion-atom collisions, Phys. Rev. A 24, 1741-1745.

Toburen LH, Ziem P, Stolterfoht N, Schneider D, Prost M. (1981b). Dynamic screening by projectile electrons in heavy ion collisions, IEEE Trans. Nucl. Sci. NS-28, 1131-1134.

Toburen LH, Wilson WE, Paretzke HG. (1982). K-Auger emission from carbon foils for 1-MeV-proton impact, Phys. Rev. A 25, 713-719.

Vriens L. (1967). Binary-encounter proton-atom collision theory, Proc. Phys. Soc. 90, 935-944.

Wilson WE. (1972). Stopping power partition and mean energy loss for energetic protons in hydrogen, Radiat. Res. 49, 36-50.

Wilson WE, Miller LH, Toburen LH, Manson ST. (1984). Differential cross sections for ionization of methane, ammonia, and water vapor by high velocity ions, J. Chem. Phys. 80, 5631-5638.

Wilson WE, Toburen LH. (1975). Electron emission from proton-hydrocarbon- molecule collisions at 0.3-2.0 MeV, Phys. Rev. A 11, 1303-1308.

Wilson WE, Toburen LH, Paretzke HG. (1978). Calculation of energy deposition spectra in small gaseous sites and its applicability to condensed phase. In: Sixth Symposium on Microdosimetry(Booz J,Ebert HG eds.) Harwood Academic Publishers Ltd., Brussels, 239-250.

Yamazaki Y, Oda N, Yasaka A. (1984). Convoy electron production from swift $H^{\circ}$, $H^{+}$, and $H_2^{+}$ beams, Nucl. Instrum. Meth. B2, 241-244.

## Discussion with Reviewers

M.E. Rudd: When dealing with "clothed" primary ions, the term "effective nuclear charge" is used. Since the effective charge is shown to be a function of the energy of the ejected electron and also to depend on the primary energy and on the target structure, is it really a useful concept? In other words, why tie the functional dependence of the cross section on, say, secondary energy to the nuclear charge?

Author: In high-energy collisions, where ionization occurs by direct coulomb excitation, both the plane wave Born approximation (McGuire et al., 1981) and classical binary encounter theory (Vriens, 1967) provide cross sections proportional to $Z_1^2|f(k)|^2$, where $Z_1$ is the projectile charge and k is the momentum transfer. Within the Born approximation this has been extended to structured ions where it was shown that the cross section could be represented by $Z_1^2(k)|f(k)|^2$, where $Z_1(k)$ represents an effective projectile charge that is independent of the target (McGuire et al. 1981). This separability of target and projectile properties is highly desireable as it allows one to make use of the wide range of information available from bare projectile studies if the functional relationship's for $Z_1(k)$ can be determined. This concept has been quite useful in stopping power where the effective charge is a simple number representing an average over momentum transfer. Our interest has been to seek a comparable effective charge which could be described as a function of momentum transfer or, in the context of our measurements, energy transfer.

M.E. Rudd: Can you say anything about the relationship between the energy distribution of electrons ejected from foils and the distribution of energies of electrons within a solid?

Author: This could be addressed more definitively by someone more knowledgeable of the theory of electron production, but I will give my general feeling as an experimentalist. When we look at electrons ejected from a foil we are seeing not only those ejected at or near the surface, but also those produced within the solid that have undergone multiple scattering, losing energy, before exiting the surface. Thus we measure a distribution of electrons that reflects those produced and scattered within the foil as well as those originating near the surface. By performing studies in which the ion energy is varied we can alter the ratio of bulk to surface electrons and by changing surface conditions we may be able to identify those electrons coming predominantly from the surface. Thus we have some experimental tools that can help in determining the distribution of electrons from within the solid, but I don't feel experiments alone will ever be adequate to fully understand the relationship between electron distributions ejected from the foil and those within the solid. What is needed is a careful comparison between results from the theory of electron scattering, including the role of bulk and surface properties on the transport process, and the measured distributions. With such comparisons we may be able to derive reliable information on the distribution of electrons produced within the solid.

R.H. Bonham: Is there reason why proton Y(E,T) functions cannot be compared directly to electron Y(E,T) functions and if not, have such comparisons been made?

Author: There is certainly no reason that the Rutherford ratios represented by Y(E,T) cannot be used to compare electron and proton impact ionization data. In fact this has been done by Kim and his coworkers; see for example Kim and Noguchi (1975). One should note however, that in the case of electron impact the ratio should be taken to the Mott formula, which includes exchange effects, rather than the Rutherford formula (Kim, 1975). If one plots Y(E,T) for protons and electron impact as a function of R/E, than equal areas under the curve contribute equally to the total ionization cross section. Compared in this way one is able to see results of exchange effects in electron impact and the greater range of momentum transfer available to equal velocity protons owing to their greater mass.

R.H. Ritchie: What cross sections were used in the Monte Carlo calculations for electron production in carbon foils? Are cross sections available for carbon targets?

Author: The cross section used in the Monte Carlo codes in our work were from a model based on the data shown in Figs 6-8 of the manuscript. The data for electron energies greater than about 30 eV are relatively insensitive to target properties other than the number of loosely bound electrons per target atom/molecule and the position of the Auger electron emission peaks. For the carbon target the differential cross sections per loosely bound electron were scaled to 4 loosely bound electrons per target atom and the Auger peak energy was taken to be 250 eV. For the Monte Carlo calculations we have performed, electron energies less than 30 eV have not been followed, thus target properties are less significant To my knowledge there are no direct experimental measurements of the single collision cross section

for electron production from carbon, either in solid form or as single atoms.

J. Schou: Are you able to derive from your measurements how much of the stopping power is caused by energy loss to ionization and to kinetic energy of the secondary electrons? How does the remaining fraction, i.e., the energy loss to excitations, depend on the primary energy?
Author: These fractions are readily available from analysis of the measured differential ionization cross sections and a knowledge of the total stopping power. A paper by Wilson (1972) described the mathematical procedure for this analysis and showed that, in the case of a hydrogen target, about 60% of the energy loss by protons with energies from 0.15 to 1.5 MeV goes into kinetic energy of the first generation secondary electrons produced. In the same energy range, about 25% of the energy lost goes into overcoming the electron binding energy in ionizing collisions and about 15% goes into producing excitation. It should be noted that the excitation fraction obtained in this way has relatively large uncertainties since it is obtained by subtraction of the major contribution to stopping power, and that contribution may have experimental uncertainties as large as 20%. The various components of stopping power derived from this analysis are nearly independent of proton energy above about 150 keV.